Size Separation of Rubber Particles from Natural Rubber Latex by Hydrocyclone Technique
Proceedings of European Congress of Chemical Engineering (ECCE-6)
Copenhagen, 16-20 September 2007

Size Separation of Rubber Particles from Natural Rubber Latex by Hydrocyclone Technique

K. Pana-Suppamassadu,[a*] S. Amnuaypanich,[b]

[a]*Department of Chemical Engineering, King Mongkut's Institute of Technology North Bangkok, 1518 Piboonsongkhram Rd., Bangsue, Bangkok 18000, Thailand*
[b]*Department of Chemistry, Khon Kaen University, 123 Mitraphrab Rd., Muang, Khon Kaen 40002, Thailand*

Abstract

In this research, the Reitema's optimum design hydrocyclone with a diameter of 8 mm was adopted to classify the size of rubber particles from NR latex. The feed pressure affected an efficiency of the separation, and the effective size separation occurred over the range of feed pressure approximately from 0.3–0.6 MPa. With a feed concentration of 0.05%, the maximum effective separation interval was 200 nm occurred at the feed pressure of 0.5 MPa. The feed concentration of the rubber latex did not significantly affect the separation performance. However, the estimated reduced cut size from the flow simulation and the semi-empirical model suggested that the operating feed pressure should be very high whereas the feed concentration should be very low in order to compensate the fact that the sizes of rubber particle are in a submicron range. This may also mean the pre-treatment of the rubber particles prior to the feeding into the hydrocyclone system is necessary. From the simulation using a finite element method (COMSOL Multiphysics), flow topology illustrated a distinct variation within the same range of feed pressure operated in this study. The flow patterns within series configurations i.e., the overflow-to-feed (OTF) and the underflow-to-feed (UTF) were also numerically studied for the first time. The flow field within the OTF was distinct from that of the UTF. A particle tracing showed the trend of very small particles reporting to the overflow, while relatively large particles reporting to the underflow.

Keywords: natural rubber, size separation, hydrocyclone, reduced cut size, particle tracing

1. Introduction

Traditionally, hydrocyclones have been widely used in mineral processing industry to separate solid particles from liquids by a force field induced by swirl flow of tangentially fed slurry mixture (Lynch et al., 1974, 1975; Trawinski, 1995). The hydrocyclone applications can be categorized as suspension concentration, liquid

clarification, thickening, classification, sorting of solid by size and density, liquid-liquid separation, and liquid-gas separation. In the past, many researchers investigated working principles of hydrocyclones in order to improve their capacity. Even though, originally, hydrocyclones have been designed to operate in solid-liquid separation, they are used in conventional solid-solid (Klima and Kim, 1998), liquid-liquid (Moraes et al., 1996) and gas-liquid separations (Marti et al., 1996) nowadays.

In the last two decades, the use of hydrocyclones in solid-liquid separations involving biology materials has been investigated. They have been used in food industry for starch refining, and as multi-stage separator systems for soluble coffee production (Ortega-Rivas, 2004). In addition, hydrocyclones have been used to separate yeast cells in continuous yeast cell cultivation and in beer industry (Seccombe, 1991; Yuan et al., 1996). Cillers and Harrison (1997) investigated the several parameters such as pressure, temperature affecting the performance of mini-hydrocyclones, namely, the recovery and concentration of yeast cells.

Many industries have had increasingly adopted mini-hydrocyclones e.g., 10 mm diameter in performing difficult phase separations. Furthermore, these hydrocyclones also have the potential to be applied to fine particle $(<10\mu m)$ suspensions classification especially to collect the sub-micron fraction. The important parameters affecting the dewatering and classification performance of 10 mm hydrocyclones are the operating pressure and feed solids concentration, both of which have previously been investigated in detail (Cilliers et al., 2004). The separation efficiency can be determined primarily by the cut size, the bypass and the water recovery to underflow.

Recently, the powerful computational fluid dynamics or CFD provides insights of fluid flow inside hydrocyclones, and the separation mechanism and performance (Dai et al., 1999; Nowakowski et al., 2004; Narasimha et al., 2005). Medronho et al. (2005) conducted the computation study to investigate the separation of microorganisms and mammalian cells. In that study, the presence of a cylindrical air core caused by the low pressure central portion occupying the whole length of hydrocyclone was observed.

In separation process, two important stages can be distinguished, i.e., separation of particles from the main swirling flow and their migration to the boundary layer on the hydrocyclone wall, and the removal of the separated particles from the wall into the apex and out of the hydrocyclone; most of particles will go through the outer vortex under the influence of centrifugal forces provided that the centrifugal forces must be greater than the drag forces, otherwise they tend to move inward in the radial direction. The separation performance of the hydrocyclones can be strongly dependent on the particle size because centrifugal and drag forces are proportional to particle volume and size, respectively.

To date, two major theories applied for the particle separation process within the hydrocyclones, i.e., the equilibrium orbit and the residence time theories.

Equilibrium Orbit Theory This theory is based on the concept of equilibrium radius of the particle, since the motion inside the hydrocyclone is developed by the swirling liquid flow itself. The radial fluid velocity toward the center and the tangential velocity are both assumed to vary exponentially with radius:

$$v_R = \frac{const}{r^m} \tag{1}$$

$$v_T = \frac{const}{r^n} \tag{2}$$

If Stokes' law is assumed, then

$$v_R = \tau \frac{v_T^2}{r} \tag{3}$$

where τ can be obtained from $$\tau = \frac{\rho_S d^2}{18\mu} \tag{4}$$

and d is a diameter of particle, and μ is the dynamic viscosity of carrier fluid. The equations can be combined to give, at equilibrium $d^2 = r^{1+2n-m}$. Since the exponent $1+2n-m>0$ therefore larger particles will be found close to the wall and entrained to the outer vortex swirling downwards toward the underflow outlet. Smaller particles, on the other hand, will be found toward the center and entered the inner fluid core swirling upward (Cilliers and Harrison, 1997). Nevertheless, since the residence time of most particles inside the hydrocyclones is typically short normally in millisecond, the equilibrium orbit theory has been criticized due to lack of consideration of the residence time of particles inside the hydrocyclones, i.e., it is unlikely will reach its equilibrium position. Moreover, the theory takes no account of the turbulences, which evidently affect the separation process (Svarovsky, 1984).

Residence Time Theory As proposed by Rietema (1965), it takes into account non-equilibrium conditions considering whether a specific size particle, d, will reach the hydrocyclone wall within its residence time, T, and report to the underflow, i.e.,

$$dt = \frac{2L}{v_Z D_C} dr \tag{5}$$

For the inlet diameter, D_I, the necessary velocity, v_R, is expressed as:

$$\int_0^T v_R dt = 0.5 D_I \tag{6}$$

Based on Stokes' analysis, the radial velocity in a centrifugal field of particles of the cut size is:

$$u_R = \frac{d_{50}^2 (\rho_S - \rho)}{18\mu} \frac{v_R^2}{r} \tag{7}$$

$$R_S = \frac{(\rho_S - \rho) L \Delta P}{9\rho D_I D_C v_Z} \frac{d_{50}^2}{\mu} \tag{8}$$

Based upon these bases, Cilliers and Harrison (1997) established the relationship between solid recovery, cut size, and viscosity for a single particle size as in equation (8); they also applied to mono-disperse particle in 10-mm hydrocyclones, and determined the feed pressure changes on solids recovery. For poly-disperse feed size

distribution, d is some representative size (Cilliers and Harrison, 1997). Nevertheless, the residence time theory does not take into account the so-called hindered settling, and neglect inertial effects and radial fluid flow.

Both theories were developed under the assumption that the feed suspension is diluted (excluding hindered settling). They led to the conclusion that the product of the Stokes number and the Euler number, $Stk_{50}Eu$, is constant for geometrically similar hydrocyclones. However, recently, Coelho and Medronho (2001) reported that the product $Stk_{50}Eu$ can be expected as a function of water flow ratio R_W and volumetric feed concentration $C_{\forall}$ since the feed concentration reduces the terminal settling velocities of the particles. Also, it is expected to vary with D_U or of an operational variable greatly affected by parameters D_U, such as the water flow ratio R_W. Based on experimental works of Coelho and Medronho (2001), a semi-empirical model based on dimensionless groups for Reitema's optimum design given by equations (12) – (14) was adopted in this study for analysis and verification purposes.

2. Experiments and FEM Simulations

The dimensions of Reitema's optimum design hydrocyclone is illustrated in Figure 1(a). A preliminary test was performed to observe the operating range that air core could occur as observed in Figure 1(b). The test rig used in the present study is shown in Figure 2. This rig was used for both in a single hydrocyclone arrangement and the Underflow-to-Feed and Overflow-to-Feed arrangements, i.e., two possibilities as seen in Figures 3(a, b). The samples of rubber solution collected from the overflow and the underflow outlets will be tested to determine the average particle size by Zeta Particle Analyzer.

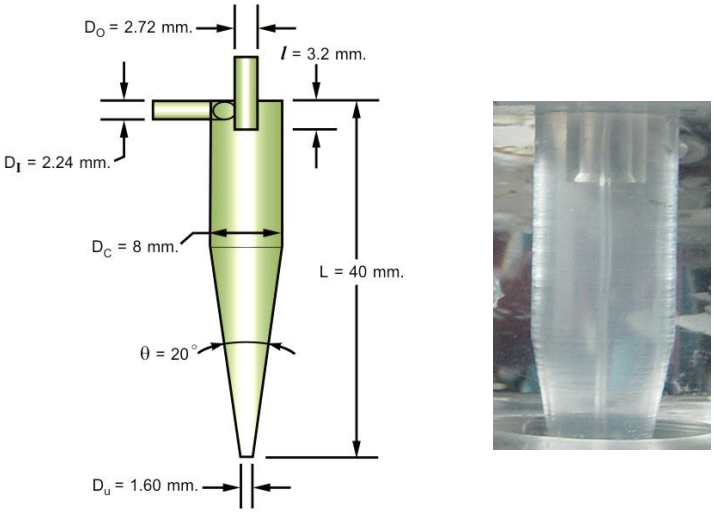

Figure 1: (a) 8-mm diameter Reitema's optimum design hydrocyclones made from acrylic adopted in the present investigation, (b) occurrence of air core.

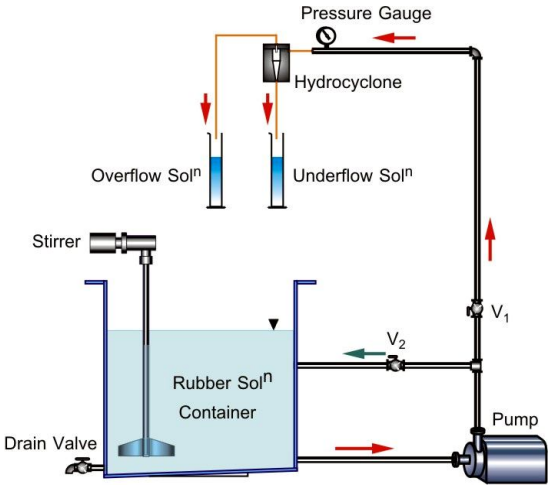

Figure 2: Test rig.

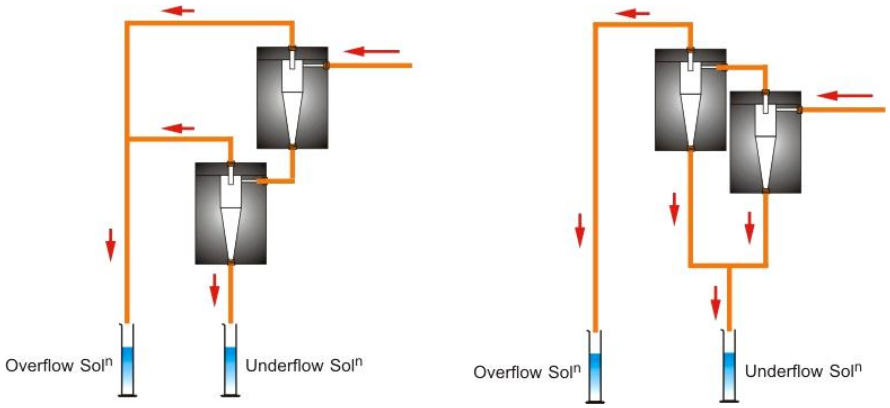

(a) (b)

Figure 3: Hydrocyclones in (a) Underflow-to-Feed (OTF), and, (b) Overflow-to-Feed (OTF) arrangements.

The simulation conducted in this investigation used COMSOL Multiphysics, which utilized the Finite Element Scheme to carry out coupled governing non-linear partial differential equations in fluid mechanics. The CFD simulation was performed with an Intel (R) Pentium (R) 4 CPU 2.93 GHz HP workstation XW8000 with 512 cache-memory, 1.00 GB RAM, and 110 GB hard disc memory. The major steps involved are explained in Figure 4, and the geometries of hydrocyclone and sets of hydrocyclones are shown in Figure 5. The underlying flow physics was also explored by the finite element method. The steady Navier-Stokes' and continuity equations are the governing equations:

$$\rho\frac{\partial\vec{u}}{\partial t}-\nabla\cdot\left[-p\tilde{I}+\mu\left(\nabla\vec{u}+(\nabla\vec{u})^{T}\right)\right]+\rho(\vec{u}\cdot\nabla)\vec{u}+\nabla p=\vec{F} \tag{9}$$

$$\nabla\cdot\vec{u}=0 \tag{10}$$

where $\vec{T} = \sigma\vec{n} = \left[-p\tilde{I} + \mu\left(\nabla\vec{u} + (\nabla\vec{u})^T\right)\right]\vec{n}$, and $\vec{K} = \tau\vec{n} = \mu\left(\nabla\vec{u} + (\nabla\vec{u})^T\right)\vec{n}$ are the total boundary and the viscous boundary force per unit area, respectively. With the governing equations, the following boundary conditions were applied: (i) normal flow/pressure $\vec{t}_1 \cdot \vec{u} = 0$, $\vec{t}_2 \cdot \vec{u} = 0$, and $\vec{n} \cdot \vec{T} = -p_o$ at the inlet; (ii) outflow/pressure $\vec{T} = -p_{atm}\vec{n}$ at the overflow and the underflow outlets; (iii) neutral $\vec{T} = \vec{0}$ between the sub-domains; and (iv) slip/symmetry $\vec{n} \cdot \vec{u} = 0$, $\vec{t}_1 \cdot \vec{K} = 0$, and $\vec{t}_2 \cdot \vec{K} = 0$ at the walls.

A particle tracing was conducted employing the Khan-Richardson force model i.e.,

$$F = \pi r_p^2 \rho \left(\bar{u} - \bar{u}_p\right)^2 \left(1.84\, Re_p^{-0.31} + 0.293\, Re_p^{0.06}\right)^{3.45} \qquad (11)$$

where $Re_p = \left|\bar{u} - \bar{u}_p\right| 2r_p\rho / \mu$. As the results, in the mean, a very small particle reported to the overflow, while a rather large particle reported to the underflow but the effective range of size separation was smaller compared to the experiments.

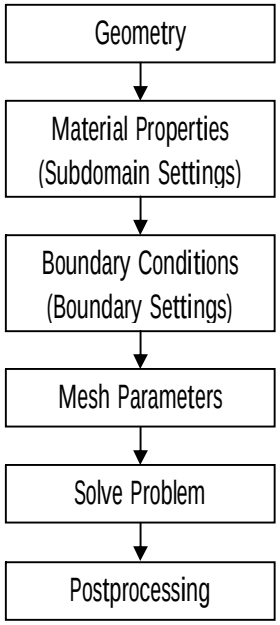

Figure 4: Procedures in flow simulation by COMSOL Multiphysics (FEM).

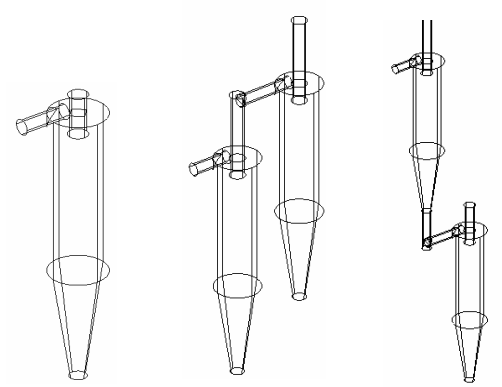

Figure 5: Geometrical models employed in the computational study: (a) Single hydrocyclone, (b) Overflow-to-Feed (OTF) arrangement, (c) Underflow-to-Feed (UTF) arrangement.

For analysis and qualitative verification purposes, the estimated cut size from the present CFD simulation was compared with that obtained from the semi-empirical correlations of Coelho and Medronho (2001). Based on experimental works and literature reviews of Coelho and Medronho (2001), a semi-empirical model based on dimensionless groups for Reitema's optimal design given by equations (12) – (14):

$$Stk_{50}Eu = 0.12\left(\frac{D_C}{D_O}\right)^{0.95}\left(\frac{D_C}{L-l}\right)^{1.33}\left[\ln\left(\frac{1}{R_W}\right)\right]^{0.79}\exp\left(12.0C_{\forall}\right) \tag{12}$$

$$Eu = 43.5D_C^{0.57}\left(\frac{D_C}{D_I}\right)^{2.61}\left(\frac{D_C}{D_O^2+D_U^2}\right)^{0.42}\left(\frac{D_C}{L-l}\right)^{0.98}Re^{0.12}\exp\left(-0.51C_{\forall}\right) \tag{13}$$

$$R_W = 1.18\left(\frac{D_C}{D_O}\right)^{5.97}\left(\frac{D_U}{D_C}\right)^{3.10}Eu^{-0.54} \tag{14}$$

where the product $Stk_{50}Eu$, the Euler number Eu, the Reynolds number Re, and the water flow ratio R_W can be found from equations (15) – (18), respectively.

$$Stk_{50}Eu = \frac{\pi\left(\rho_S-\rho\right)\Delta PD_C d_{50}'^2}{36\mu\rho Q} \tag{15}$$

$$Eu = \frac{\pi^2\Delta PD_C^4}{8\rho Q^2} \tag{16}$$

$$Re = \frac{4\rho Q}{\pi\mu D_C} \tag{17}$$

$$R_W = \frac{Q_U\left(1-C_{\forall U}\right)}{Q\left(1-C_{\forall}\right)} \tag{18}$$

The reduced grade efficiency curve G' as expressed in equation (19) was given by a modification of the Rosin-Rammler distribution function as proposed by Plitt (1976). The reduced grade efficiency and the particle size distribution of the feed as cumulative undersize fraction y as expressed in equation (20) will describe the performance of hydrocyclone (Castilho and Medronho, 2000).

$$G' = 1-\exp\left[-0.693\left(\frac{d}{d_{50}'}\right)^{2.45}\right] \tag{19}$$

$$y = 1-exp\left(-\left(\frac{d}{k}\right)^m\right) \tag{20}$$

Furthermore, the reduced total efficiency E_T' and the total efficiency E_T can be determined from equations (21) – (22).

$$E_T' = \int_0^1 G'dy \tag{21}$$

$$E_T' = \frac{E_T - R_W}{1 - R_W} \tag{22}$$

By considering equations (12) and (15), the reduced cut size as expressed in equation (23) will be calculated.

$$d_{50}' = \frac{1.173 D_C^{0.64}}{D_O^{0.475}(L-l)^{0.665}} \left[\frac{\mu\rho Q}{(\rho_S - \rho)\Delta P}\right]^{0.5} \left[\ln\left(\frac{1}{R_W}\right)\right]^{0.395} \exp(6.0 C_\forall) \tag{23}$$

3. Results and Discussion

Flow structures and flow physics within a single 8-mm hydrocyclone was explored using the COMSOL Multiphysics. Insights can be obtained from physics of the simulated flow. From the flow simulation, the performance parameters, e.g., reduced cut size, pressure drop, flow rates could be determined.

3.1. Performance of a Single Hydrocyclone

In Figure 6, the instantaneous velocity filed at the operating feed pressure of 0.7 MPa, and the corresponding streamline around the inlet of vortex finder close to the overflow outlet were displayed. The absence of short circuit of the flow and so the rubber particles passing through the vortex finder without experiencing the centrifugal separation was confirmed. As the feed tangentially enter the hydrocyclone, the axial component velocity directed the flow downward, and with a proper penetration of vortex finder used (l) thus the short circuit is avoided. Figure 7 showed the flow topology and Reynolds cell within a single 8-mm hydrocyclone at the same feed pressure. Obviously, the indication of the reverse swirling flow near the core (asymmetric axis) of flow field in the hydrocyclone is obvious. With a proper design cut size, the particles those are larger than the cut size are expected to be forced toward to the hydrocyclone wall and directed downward to the underflow exit. On the other hand, the particles smaller than the cut size are expected to flow along with the inner swirl in the core and out thru the overflow outlet.

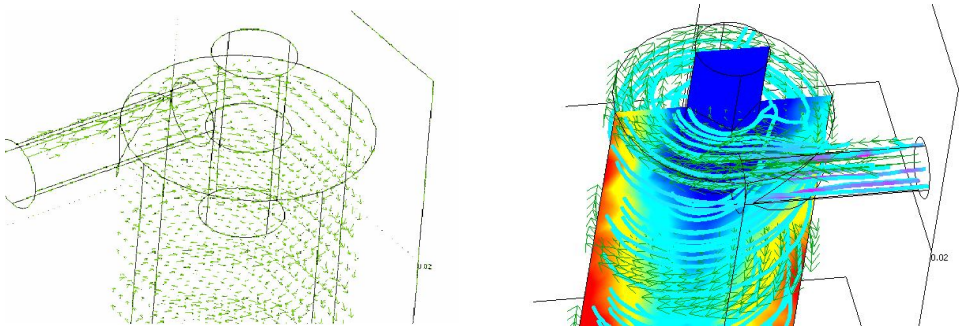

Figure 6: Instantaneous velocity vectors and corresponding streamlines in the vicinity of the vortex finder indicating no short cut is taking place (at the feed pressure of 0.7 MPa).

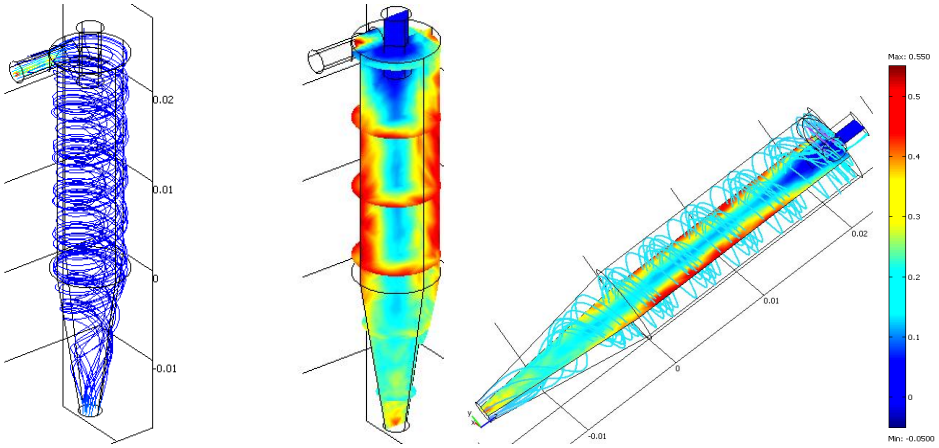

(a) (b)

Figure 7: Streamlines and Reynolds cell within a single 8 mm hydrocyclone at the feed pressure of 0.7 MPa.

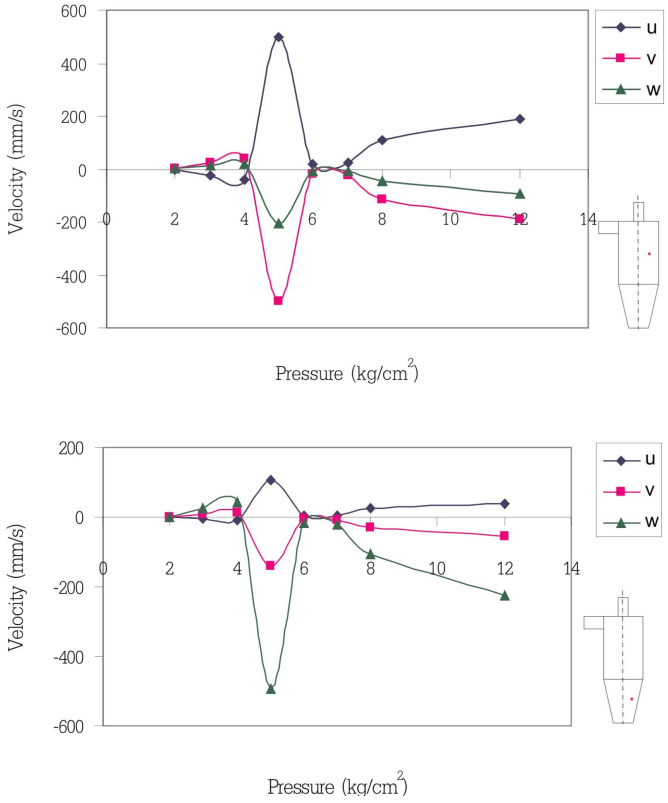

Figure 8: Velocity components within the cylindrical and conic portions of 8-mm hydrocyclone as a function the feed pressure (1 kg/cm^2 ≡ 0.1 MPa).

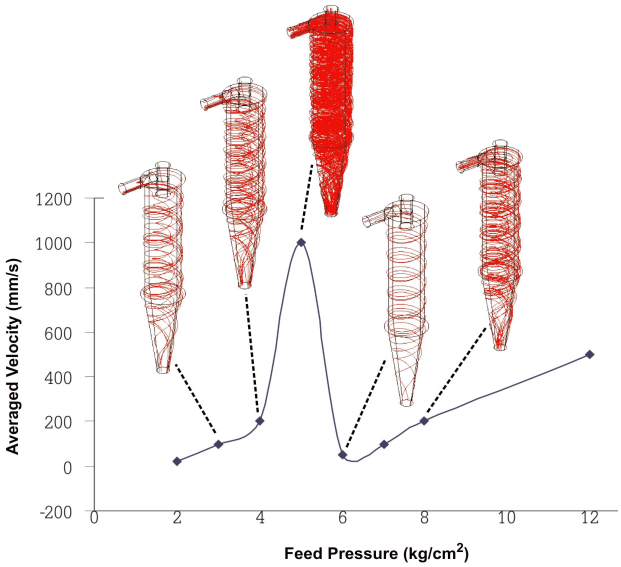

Figure 9: Averaged velocity and flow topology at various operating feed pressure.

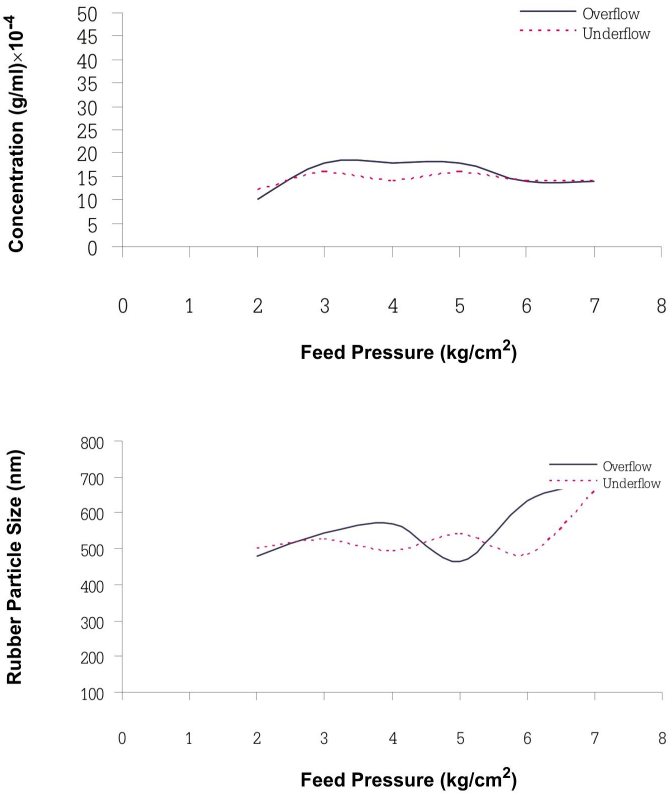

Figure 10: (a) Concentration, and (b) size separation of rubber particle fed through the hydrocyclone at various feed pressure.

The flow structure simulated exhibited organized swirl pattern within the hydrocyclone but it also exhibited a rather strong dependence on the feed pressure. Figure 8 and 9 illustrated the complex relation among the feed pressure, the velocity components, and related flow field. Both flow structures within the cylindrical and conic sections displayed a similar characteristics even though with different value of the velocity components especially the tangential velocity component. Although, the feed pressure mildly affected the performance of the hydrocyclone, and the most effective size separation occurred over the range of feed pressure approximately from 0.3–0.6 MPa, with a feed concentration of 0.05%, the maximum effective separation interval was 200 nm occurred at 0.5 MPa. Figure 10(a) showed the concentration and the size separation of rubber particles fed through the hydrocyclone at different feed pressure. It seems that the rubber particles could not be effectively separated via a single stage hydrocyclone because of their relatively very small size compared to the design reduced cut size (see section 3.2).

Similarly, the resulting concentration as shown in Figure 10(b) was not affected by the feed pressure as well. Either the force field induced by the swirling flow is not strong enough to promote the separation or the particle size is unreasonably small, the improvement of hydrocyclone system only by rearranging many hydrocyclones in series configurations seems not adequate. However, the estimated cut size from the flow simulation and the semi-empirical model (see section 3.2) suggested that the operating feed pressure should be high, whereas the feed concentration should be very low in order to compensate the fact that the sizes of rubber particle are in a submicron range. This may also mean the pre-treatment of the rubber particles prior to the feeding into the hydrocyclone system is still necessary. In addition, the feed concentration of the rubber latex did not significantly affect the separation performance as well.

3.2. Reduced Cut Size

The reduced cut size was estimated from the trajectory of particle of the size that moving approximately on the Locus of Zero Vertical Velocity (LZVV) (example of particle tracing was shown in Figure 11) and compared to that was determined from the semi-empirical model proposed by Coelho and Medronho (2001). The estimated reduced cut size from the CFD simulation and the semi-empirical formulae obtained from the linear regression of the experimental data by Coelho and Medronho

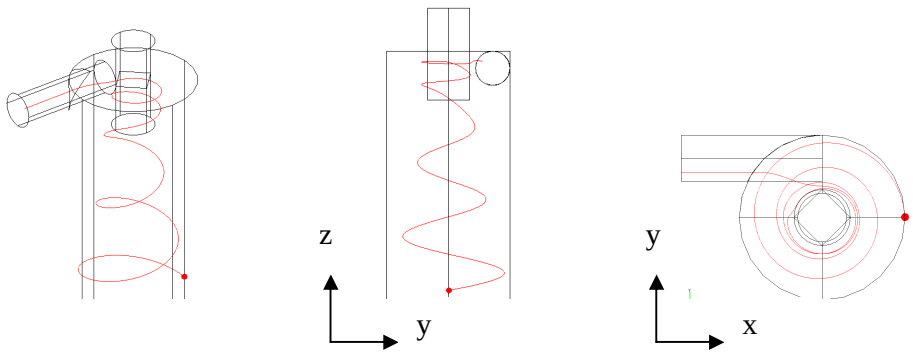

Figure 11: Particle Tracing.

(2001) were shown in Figures 12 and 13 as a function of feed pressure and feed concentration, respectively. The difference between the predicted cut size base on the semi-empirical model and the simulation may be caused by the turbulence of the flow. Turbulence played an important role in the performance of hydrocyclone (or gas cyclone) as reported in many studies (Gimbun et al., 2005; Coelho and Medronho, 2001; Ogawa, 1984). Due to the anisotropic characteristic of turbulence in hydrocyclone, the Reynolds stress turbulence model seems to yield an accurate prediction on swirl flow pattern, axial velocity, tangential velocity and pressure drop on cyclone simulation (Gimbun et al., 2005). Beside the loss due to contraction or expansion of the flow at inlet/out of the hydrocyclone, energy loss due to viscous stress of the turbulent swirling flow is responsible for difference in cut size estimation.

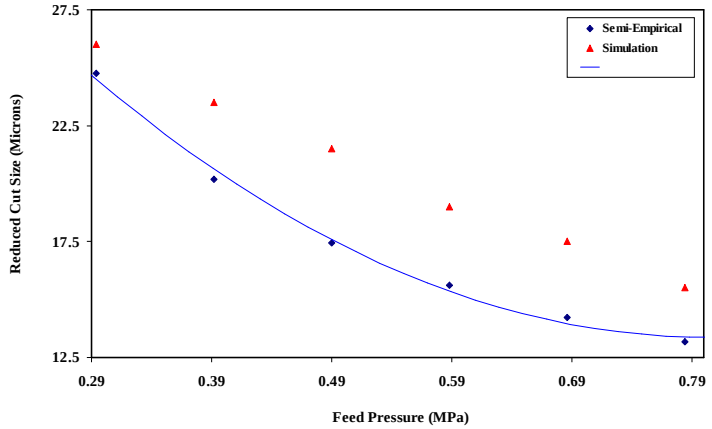

Figure 12: Reduced cut size estimated from the LVZZ as compared to the reduced cut size predicted by the semi-empirical model as a function of feed pressure.

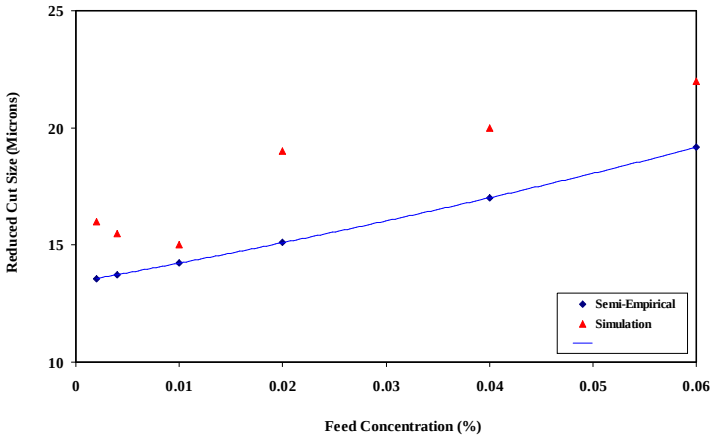

Figure 13: Reduced cut size estimated from the LVZZ as compared to the reduced cut size predicted by the semi-empirical model as a function of feed concentration.

Estimated cut size either by the flow simulation or the semi-empirical model suggests that the operating feed pressure should be high whereas the feed concentration should be kept very low to compensate the submicron size of the natural rubber particle. In addition to varying the operating conditions or pretreatment of the feed, the alternatives of arranging the hydrocyclones in series must be investigated.

3.3. Overflow-to-Feed (OTF) and Underflow-to-Feed (UTF) Hydrocyclones Arrangements

As possibilities to improve the performance of hydrocyclone, the connection of hydrocyclones in the Overflow-to-Feed (OTF) and the Underflow-to-Feed (UTF) arrangements were considered. The simulated streamlines of the OTF and UTF arrangements were demonstrated in Figures 14 and 15, respectively. For both cases, the operating feed pressures were 0.7 MPa and 1.2 MPa.

As compared to the UTF (Figure 15) arrangement, the OTF arrangement had the streamline pattern equally distributed over both hydrocyclones. However, the streamline pattern can mislead since the average energy in the followed hydrocyclone is less than that in the first hydrocyclone according to the friction, the contraction, and the expansion losses as previously mentioned. The higher power pump was required to overcome more pressure drop across both hydrocyclones. The feed pump must also be powerful enough to produce the necessary intense force field on the second hydrocyclone.

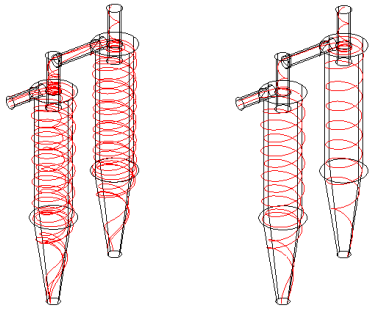

(a) (b)

Figure 14: Streamlines of the Overflow-to-Feed (OTF) hydrocyclone arrangement at the operating feed pressure (a) 0.7 MPa, and (b) 1.2 MPa.

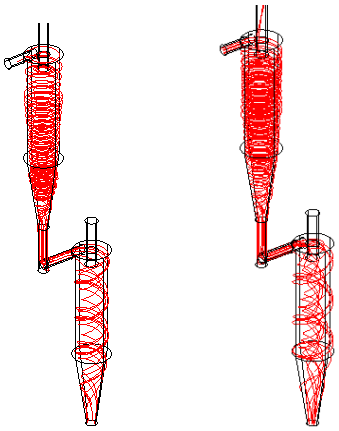

(a) (b)

Figure 15: Streamlines of the Underflow-to-Feed (UTF) hydrocyclone arrangement at the operating feed pressure (a) 0.7 MPa, and (b) 1.2 MPa.

4. Conclusions

The performance of Reitema's hydrocyclone in size separation of natural rubber particles was not adequately effective since the average size of the rubber

particle is much smaller than the design cut size as indicated by the simulation or the semi-empirical formulae. Therefore, the size separation of natural rubber particles may need a pre-treatment prior to be fed through the hydrocyclone systems. Further work is required on this subject. However, the estimated cut size suggested that the operating feed pressure should be high, whereas the feed concentration should be very low in order to compensate the fact that the sizes of rubber particle are in a submicron range.

Acknowledgement

The authors gratefully acknowledge the Thailand Research Fund (TRF) for part of the financial support.

References

Castilho, L.R. and Medronho, R.A., (2000), *Minerals Engineering*, 13, 183-191.

Cilliers, J.J., Diaz-Anadon, L. and Wee, F.S., (2004) *Minerals Engineering*, 17, 591-597.

Cilliers, J.J., Harrison, S.T.L., (1997) *Chemical Engineering Journal*, 65, 21-26.

Coelho, M.A.Z. and Medronho, R.A., (2001) *Chemical Engineering Journal*, 84, 7-14.

Crowe, C., Sommerfeld, M. and Tsuji, Y., *Multiphase Flows with Droplets and Particles*, CRC Press, USA (1998).

Dai, G.Q., Li, J.M. and Chen, W.M., (1999) *Chemical Engineering Journal*, 74, 217-223.

Gimbun, J., Chuah, T.G., Fakhru'l-Razi, A. and Choog T.S.Y., (2005) *Chemical Engineering and Processing*, 44, 7-12.

Klima, M.S. and Kim, B.H., (1998) *Journal of Environmental Science and Health*, A33, 1325-1340.

Lynch, A.J. and Rao, T.C. and Bailey, C.W. (1975) *International Journal of Mineral Process*, 2, 29-37.

Lynch, A.J. and Rao, T.C. and Prisbrey, K.A. (1974) *International Journal of Mineral Process*, 1, 173-181.

Marti, S, Erdal, F.M., Shoham, O., Shirazi, S. and Kouba, G.E., (1996) *Hydrocyclones*, London & Bury Saint Edmunds: Mechanical Engineering Publication, 339-421.

Medronho, R.A., Schuetze, J. and Deckwer, W-D., (2005) *Lat. Am. App. Res.*, 35, 1-8.

Moraes, C.A.C., Hackenburg, C.M., Russo, C. and Medronho, R.A., (1996) *Hydrocyclones*, London & Bury Saint Edmunds: Mechanical Engineering Publication, 339-421.

Narasimha, M., Sripriya, R. and Banerjee, P.K., (2005) *International Journal of Mineral Processing*, 75, 53-68.

Nowakowski, A.F., Cullivan, J.C., Williams, R.A. and Dyakowsi, T., (2004) *Minerals*

Engineering, 17, 785-790.

Ogawa, A., *Separation of Particles from Air and Gasses,* Vol. 1.&2, CRC Press, USA (1984).

Ortega-Rivas, E., (2004) *Eng. Life Sci.,* 4, 119-123.

Plitt, L.R., (1976) *CIM Bull.,* 69, 114-123.

Rietema, K., (1965) *Chem. Eng. Sci.,* 15, 298-325.

Seccombe, P., (1991) *J. Chem. Tech. Biotech.,* 51, 284-285.

Svarovsky, L., *Hydrocyclones,* Holt: Reinehart and Winston Ltd., (1984).

Wolbert, D., Ma, B.-F., Aurelle, Y. and Seureau, J., (1995) *AIChE Journal,* 41, 1395-1402.

Yuan, H., Rickwood, D., Smyth, I.C. and Thew, M.T., (1996) *Bioseparation,* 6, 159-163.